Integrated Experimental And Numerical Study To Evaluate The Performance Of A GI Runner For Archimedes Screw Turbine

Tanish Kashyap[1*], Robin Thakur[2]

[1,2]School of Core Engineering, Shoolini University, Solan-173229 (HP) India

Abstract –
Micro-hydropower has gained attention in recent years with growing interest in low-head turbines due to their efficiency, cost effectiveness and ability to operate at low flow rates with minimal environmental impact. Among these systems the Archimedes screw turbine (AST) is a promising option for supplying electricity to rural and remote areas. This study investigates the performance of an AST fabricated with a galvanized iron (GI) runner through laboratory experiments and CFD modelling. Experiments were conducted at inclination angles between 20° and 40° with flow rates of 1-5 $kg{\cdot}s^{-1}$. Parameters such as torque, rotational speed, output power and hydraulic efficiency were evaluated and the maximum efficiency of 72.51% was recorded at 20° inclination angle and 1 $kg{\cdot}s^{-1}$ flow rate. A three-dimensional CFD model was developed in ANSYS fluent using a polyhedral mesh, Eulerian multiphase approach and the realizable k–ε turbulence model. The numerical predictions matched closely with experimental results showing a peak efficiency of 70%. Pressure contours and transient flow fields provided insight into flow behaviour. Results highlight GI as a practical and durable runner material for AST in rural low-head micro-hydropower systems.

Keywords: Archimedes screw turbine, Runner material, Flow rate, Computational fluid dynamics, Micro-hydropower.

1. Introduction

Energy is essential for economic and social growth and is vital for all human activities [1]. Conventional sources like coal and petroleum are limited in supply and highly polluting which makes the use of renewable energy resources necessary [2,3]. Renewable sources such as hydropower, solar, wind, biomass and geothermal offer clean and sustainable alternatives [4–6]. However, their utilization depends on geographical and climatic conditions. Solar energy is often available for a short period during cloudy or rainy weather [7–10] and is available in two forms like solar thermal which heats working fluids [11–13] and photovoltaic systems which generate electricity [14–15]. Wind energy also varies with regional climate. Thermal and nuclear energy are strongly discouraged due to their severe environmental impacts and association with human health risks.

Hydropower remains the most reliable renewable energy source because it uses water that is running or stored [16-19]. However, large projects can have negative effects on the environment [20-22], as Xiao et al. [23] found that the Ertan hydropower station caused erosion and habitat degradation. Li et al. [24] found a similar result in the Jinsha River basin as such projects disturb the balance of nature. Micro-hydropower systems on the other hand provide local and environmentally safe energy options that can be without undue disturbance to the environment. These systems have a water source, turbine and generator where the turbine converts energy of water into mechanical power and generator transforms this mechanical energy into electrical energy [25-27]. Khan et al. [28] found that micro-hydropower systems in rural Pakistan could provide clean and low-cost energy with less emissions. In a similar study, Triana et al. [29] found that micro-hydropower system could be a better option for rural communities in Indonesia leading to environmentally beneficial practices.

Turbine for power generation comes in several varieties that can be used to produce energy such as impulse, reaction and gravity turbines [30-32]. Among these, Archimedes

screw turbine is one type that is of particular interest due to its simple design, long life and efficiency in low-head situations [32]. ASTs are friendly for aquatic organisms like fish as it can pass through the turbine without getting serious injuries. It is suitable for rural regions where the installation of other types of turbines is expensive both in installation and maintenance costs [33–35]. Based on this, Helmizar et al. [36] examined the suitability of AST for small head locations through laboratory tests. The study found that smaller inclination angle help in assisting water filling with reduced slippage and enhanced hydraulic energy. The primary focus of the study was the design optimization in order to improve turbine performance. Further, Indarto et al. [37] observed that parameters such as the blade number, inclination angle and shaft length strongly influence the efficiency. While, Maulana et al. [38] used CFD model to validate that AST can sustain rotation even when heads are below one meter with double screw designs performing best at higher flows. Darmono and Pranoto [39] observed that variations in thread number significantly affect torque, power and pressure drop, highlighting the significant role of screw geometry. Uniyal et al. [40] revealed that artificial neural networks exceed response surface methodology in performance prediction yielding greater accuracy in turbine simulation. AST was chosen to be ideal solution for rural application owing to its adaptability and minimal environmental impact. Imawati et al. [41] developed a pico-hydro AST designed to operate under varying flow rates in order to achieve stable output with simple design and ease of installation. Muzaka et al. [42] and Edirisinghe et al. [43] demonstrated that performance of AST is strongly dependent on the angle of inclination achieving better output even at 45°. Economically, Zamani et al. [44] used a genetic algorithm to optimize the AST design and observed payback periods ranging from 2.55 to 5.93 years confirming its economic feasibility. The choice of material also affects the durability and performance of AST as it influences corrosion resistance, efficiency and frictional losses. According to experimental study by Kashyap et al. [45] stainless steel lowers friction and prevents rusting and found that more than 70% of conventional water mill locations are appropriate for AST installations. Further, a mild steel design was tested under low flow conditions by Lee and Lee [46] who also developed regression models connecting torque, RPM and inclination angles thereby, finding a good correlation value of more than 60%. Mild steel AST were tested by Abbas et al. [47] using CFD and experimental models which revealed deviations of less than 5%. In a 3D RANS-based CFD model, Shahverdi et al. [48] employed smooth steel and attained an overall efficiency of 83%. According to Abdullah et al. [49] a stainless-steel AST was used at different flow rates and inclination angles which resulted in an increase in efficiency of 81%.

Overall, existing research highlights the effectiveness and environment sustainability of AST for low head hydropower applications. To enhance energy capture and efficiency most studies focus on the optimizing key parameters such as the inclination angle, blade number, screw length and overall geometry. Material selection also plays a vital role in minimizing friction and corrosion losses, improving durability and performance. However, limited studies have explored alternative materials that offer similar efficiency at lower cost with better corrosion resistance. Furthermore, few studies combine experimental and numerical analyses to examine internal flow behaviour and only a small number validate CFD models against experimental results for greater accuracy. To address these research gaps the study aims to,

1) To design and test a galvanized iron Archimedes screw turbine for low-head hydro-power use.
2) To create a CFD model of the turbine and validate its performance by comparing simulation results with experimental data.

2. Methodology

This study adopts a combined experimental and numerical approach to evaluate the performance of an AST equipped with GI runner. The methodology involves the design and manufacturing the turbine, experimental testing under controlled conditions, computational fluid dynamics simulation and validation.

2.1 Experimental setup and parameters

The equipment was fabricated at the lab scale to test the performance of the device in controlled conditions. A control valve regulated the flow of water pumped from a storage tank to the turbine, with a flow meter monitoring the flow rate. The flow behaviour and operational characteristics of the screw turbine setup were designed in accordance with the analytical model presented in [50], which provides equations for estimating the flow volume through AST under varying operating conditions. The overall schematic diagram and the actual laboratory set up used for testing is shown below in Figures 1 and 2. The speed of the turbine was noted by a digital tachometer and the torque was calculated by a rope-brake mechanism consisting of a 0.1m diameter drum and 0.0064 m diameter rope. The turbine used a GI steel runner coated with protective paint to resist corrosion and improve durability. Screw inclination was adjusted with an angle gauge for precise positioning.

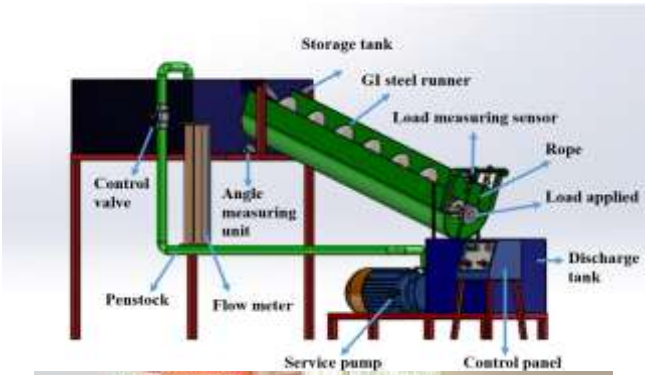




Fig. 1. Schematic view of setup. *Fig. 2. Actual view of setup.*

The effect of inclination angle on the AST performance was examined in [51,52], indicating both the pitch ratio and inclination testing are necessary for power output and efficiency outcome. In references [53,54], it was discovered that changes in head had an impact on both torque and total energy output, highlighting the impact of head on the torque performance. In order to assess their combined impact on the turbine efficiency, head, flow rate and inclination angle were all considered in the study. To ensure accurate and consistent results, four set of readings were taken at two-hour intervals for each

variation in flow rate and inclination angle. The main parameters used in the experiment are shown in Table 1.

Table 1. Experimental parameters undertaken for setup.

Parameters	Symbol	Range
Screw turbine length	S_{length}	1.65 m
Pitch	P_{itch}	0.06 m
Head	H_{ead}	0.56, 0.70, 0.83, 0.95, 1.06 m
Angle of inclination	I_{angle}	20°, 25°, 30°, 35°, 40°
Inner diameter of turbine	D_{inner}	0.1 m
Outer diameter of turbine	D_{outer}	0.2 m
Load	L_{oad}	0.7, 0.8, 0.9, 0.95, 1.0 kg
Diameter of rope	D_{rope}	0.0064 m
Brake drum diameter	D_{brake}	0.1 m
Flow rate	F_{rate}	1-5 $kg{\cdot}s^{-1}$
Density of water	ρ_{wa}	997 kg/m^3

2.2 Calculation method:

1. Turbine Efficiency (η): The efficiency of the AST is the ratio of output power to input power. It reflects how effectively the turbine converts hydraulic energy into mechanical energy. The formula used is:

$$\eta = \left(\frac{P_{out}}{P_{in}}\right) \times 100 \quad (1)$$

2. Input Power (P_{in}): This is the theoretical hydraulic power available based on the head and discharge. It is calculated assuming no losses. The formula is:

$$P_{in} = \rho_w \times g \times H_{ead} \times Q_d \ (Kw) \quad (2)$$

where, $\rho_w = Density\ of\ water\ \left(997 \frac{kg}{m^3}\right)$

$g = Gravitational\ constant\ (9.81\ \frac{m}{s^2})$

$H_{ead} = Height\ of\ water\ column.$

$Q_d = Discharge\ rate$

3. Output Power (P_{out}): This is the actual power output from the turbine. It is based on the rotational speed and torque produced by the turbine and is given by:

$$P_{out} = \frac{2 \times \pi \times n \times T}{60} \ (Kw) \quad (3)$$

where, $n = Rotational\ speed\ (RPM)$

$T = Torque$

4. Torque (T_{orq}): Torque is the rotational force generated by the load applied on the turbine. It is calculated using the formula:

$$T_{orq} = L_{oad} \times g \times R_e \quad (4)$$

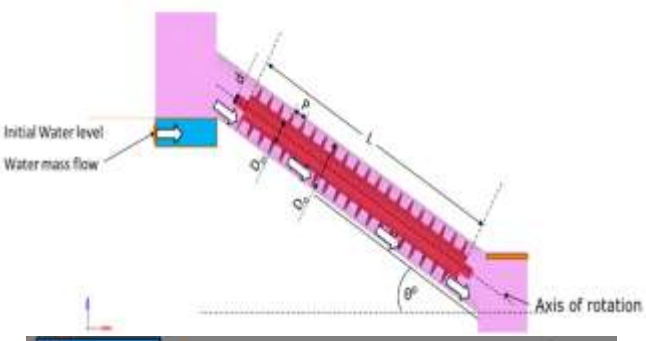
$L_{oad} = Applied\ load\ in\ Kg$

$g = Gravitational\ constant\ (9.81\ \frac{m}{s^2})$

$R_e = (Br_{dia} \times 2\ \frac{Dia_{rope}}{2})\ \ (m)$

2.3 Computational modelling and analysis

The hydraulic and mechanical performance of the AST with different flow conditions was analysed through CFD simulations. The turbine geometry was made in Creo based on the experimental set-up and imported to ANSYS Workbench for pre-processing. To effectively capture the interaction between the flowing water and the screw blades, the computational domains were defined. Mesh refinement was carefully applied in regions with high velocity gradients like blade edges and shaft interface to ensure grid independence and maintain high element quality. The implemented meshing strategy ensured accurate capture of the complex flow behaviour within the screw channel and improved numerical stability. The CFD modelling process including preparation of geometry and mesh generation is illustrated in Figures 3 and 4 respectively.



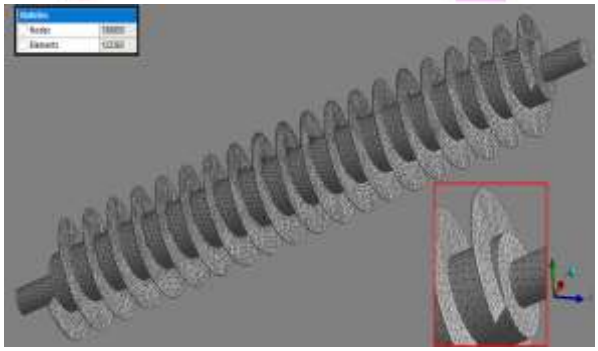


Fig. 3. Runner geometry for AST. ***Fig. 4. Final 3D meshed geometry***

The final meshed model made of about 1,98,800 nodes and 1,22,363 elements ensured a good balance between computational efficiency and precision. Further, the boundary conditions were defined as a velocity inlet and a pressure outlet. The rotating region was adjusted with a user-defined function (UDF). This function altered the angular velocity on the basis of residual torque. The simulation used a 3D transient solver with Eulerian multiphase model, realizable k–ε turbulence model and SIMPLE pressure-velocity coupling. The present CFD methodology follows the approach outlined in [55, 56], where numerical models were validated against laboratory-scale experiments to accurately predict flow distribution and energy conversion in AST. The parameters for the CFD modelling are summarized in Table 2.

Table 2. CFD modelling parameters

Parameter	**Setting**
Solver Type	Pressure-based solver
Flow Type	Transient (time-dependent) simulation
Multiphase Model	Eulerian multiphase model (two phases: water and air)
Primary Phase	Air

Secondary Phase	Water
Phase Interaction	Interfacial drag with standard drag laws (if defined)
Turbulence Model	Realizable k-ε with scalable wall functions and curvature correction
Pressure-Velocity Coupling	SIMPLE (Semi-Implicit Method for Pressure-Linked Equations)
Pressure Interpolation	Second-order
Discretization – Momentum	Second-order upwind
Transient Formulation	Bounded second-order implicit (ensures temporal stability and higher accuracy in unsteady flows)

3. Results and Discussion

Evaluating key performance parameters is essential for optimizing the efficiency and reliability of AST. Each parameter has a different role in determining the energy conversion efficiency and the performance of the turbine. The first parameter to consider is the flow rate, which defines the volume of water that flows into the screw and has a direct impact on the torque, rotational speed and power output produced by the turbine. The head represents the available hydraulic energy which has an influence on both the turbine load and the potential energy input. The torque tells us how much rotational force is produced by the water on the screw blades and angular velocity measured in RPM indicates the rotational response of the turbine. The power output indicates the total mechanical energy produced and is the result of torque and speed outputs.

The efficiency is the final outcome parameter that indicates the extent of hydraulic energy conversion into mechanical output. In addition to validating and identifying potential operational conditions for small scale hydropower, experimental testing and CFD modelling of these variables allow for accurate performance prediction. This section presents the experimental and CFD results of an AST equipped with a GI runner and the comparison between them. The important aspect in this analysis is that the flow, head and angle of inclination each have an effect on the key performance parameters of torque, angular velocity, power output and efficiency. The strong agreement between the experimental and CFD results shows that both are reliable methods and validates the accuracy of the simulation approach. The detailed values obtained from both experimental work and CFD simulations for different angles of inclination are presented in Table 3.

Table 3. Experimental and CFD Results at different inclination angles.

Inclination angle (°)	**Flow rate (kg. s^{-1})**	**Head (m) (Exp)**	**Head (m) (CFD)**	**Torque (N-m) (Exp)**	**Torque (N-m) (CFD)**	**Angular velocity (RPM) (Exp)**	**Angular velocity (RPM) (CFD)**	**Power output (W) (Exp)**	**Power output (W) (CFD)**	**Efficiency (η) (Exp)**	**Efficiency (η) (CFD)**
20°	1	0.56	0.57	0.412	0.42	92.1	88.32	3.9715	3.88	72.51	70.00
25°	1	0.70	0.71	0.470	0.47	94.2	93.02	4.6340	4.58	67.68	66.00

30°	1	0.83	0.85	0.529	0.52	99.1	99.36	5.4870	5.41	65.21	65.00
35°	1	0.95	0.94	0.559	0.55	102.5	102.28	5.9971	5.90	64.54	63.50
40°	1	1.06	1.05	0.588	0.58	105.9	105.20	6.5175	6.39	62.86	62.00

3.1 Graphical Comparison of Experimental and CFD Results

The computational model was validated and comparative graphs were generated to visually examine the agreement between the experimental and simulated results of the AST with a galvanized iron runner. These graphs show how torque, angular velocity, power output and efficiency change with inclination angle based on the experimental and CFD analysis.

3.1.1 Effect of Flow Rate on Power Output

Increasing the flow rate results in higher power output for all inclination angles in both experimental and computational analyses. Among all configurations tested, higher angles produce larger outputs and lower angles produce less output as can be seen in Figures 5 and 6. This indicates that more energy is converted at higher angles because of greater hydraulic head and torque.

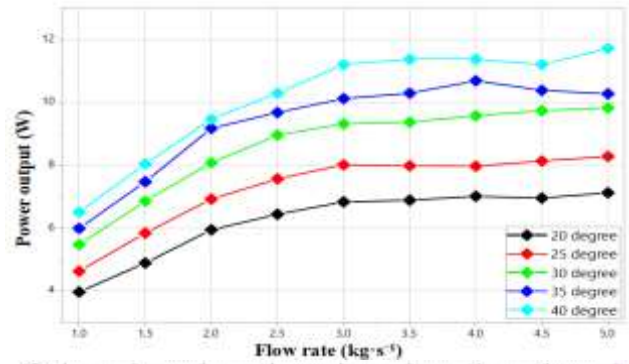


Fig 5. Flow rate vs power output (Experimental).

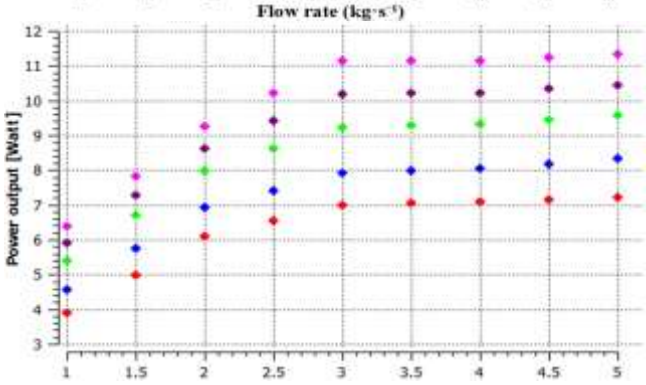
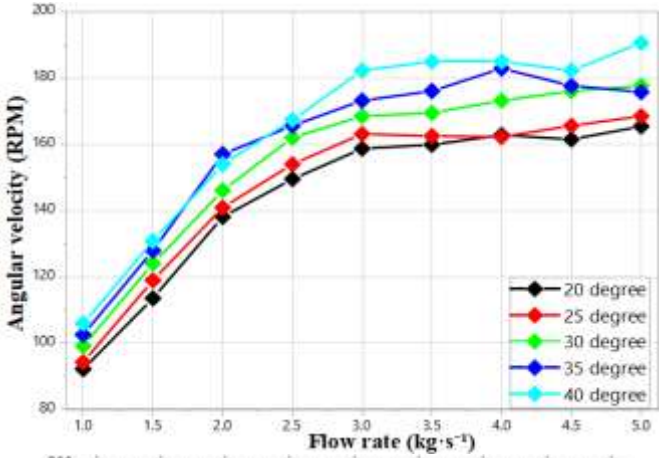


Fig 6. Flow rate vs power output (CFD).

3.1.2 Effect of Flow Rate on Angular Velocity

The angular velocity progressively increases with increasing flow rate for all angles of inclination in both experimental and CFD analysis. A greater angle of inclination results in a higher velocity of rotation. This is due to the increased hydraulic head and torque being produced with the greater angles of inclination while the smaller angles produce lower rates of rotation as can be seen in Figures 7 and 8. This agreement between the

experimental and CFD findings confirms the accuracy and reliability of the numerical model in predicting the rotational characteristics of the AST constructed from galvanized iron runner under the different flow conditions.



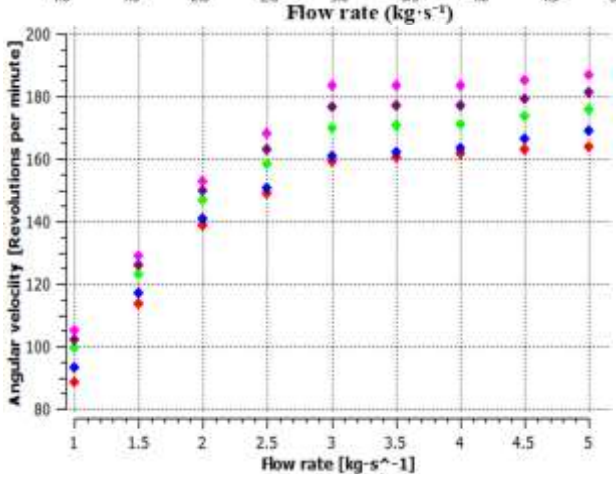
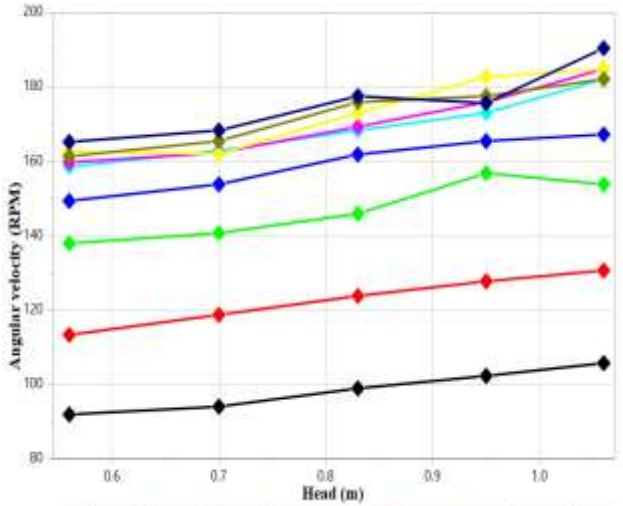


Fig. 7. Flow rate vs Angular velocity (Experimental). Fig. 8. Flow rate vs Angular velocity (CFD).

3.1.3 Effect of Head on Angular velocity

The angular velocity increases with increasing hydraulic head, which reflects a greater transfer of energy from the water to the turbine shaft. The CFD results show a similar trend, which closely aligns with experimental data and validates the numerical model as shown in Figures 9 and 10.



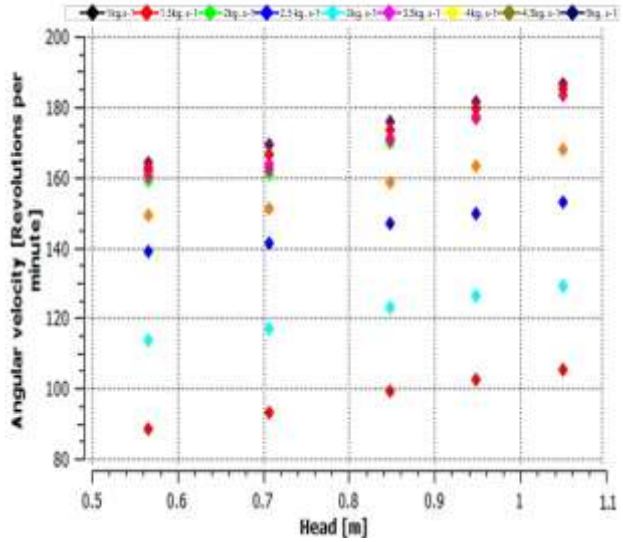
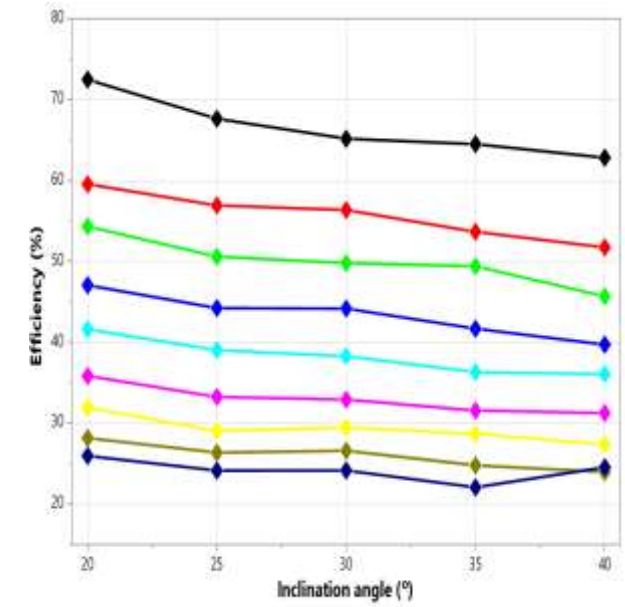


Fig. 9. Head vs Angular velocity (Experimental).

Fig. 10. Head vs Angular velocity (CFD).

3.1.4 Effect of inclination angle on Efficiency

The efficiency decreases gradually with increasing angle of inclination showing that small angles favour promising hydraulic behaviour. The CFD analysis exhibited similar results to that observed in the experimental findings with good agreement and validating the numerical model for predicting the efficiency behaviour as depicted in Figures 11 and 12. Overall, both analyses indicate that the GI runner exhibits higher efficiency for moderate angles of inclination.



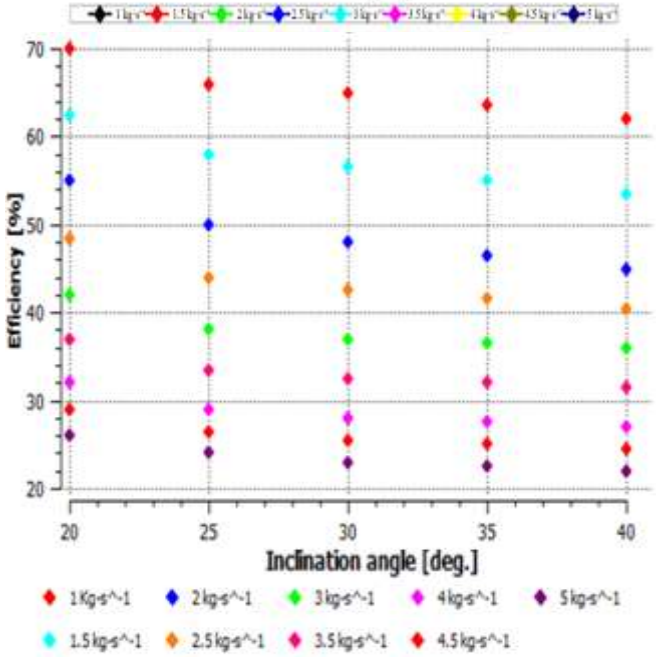
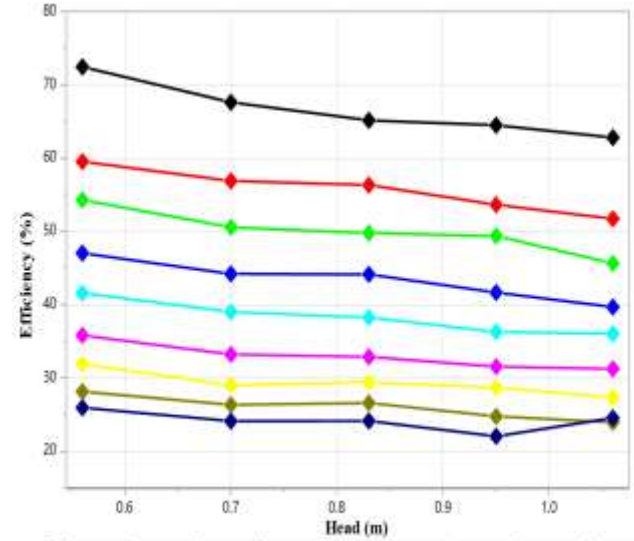


Fig. 11. Inclination vs Efficiency (Experimental).

Fig. 12. Inclination vs Efficiency (CFD).

3.1.5 Effect of Head on Efficiency

The efficiency slightly decreases with increasing head which means energy losses are greater at larger heads. The CFD results showed a similar pattern in accordance with the experimental results. Overall, both analyses confirm that efficiency is generally stable at lower heads where the turbine works more efficiently as shown in Figure 13 and 14.



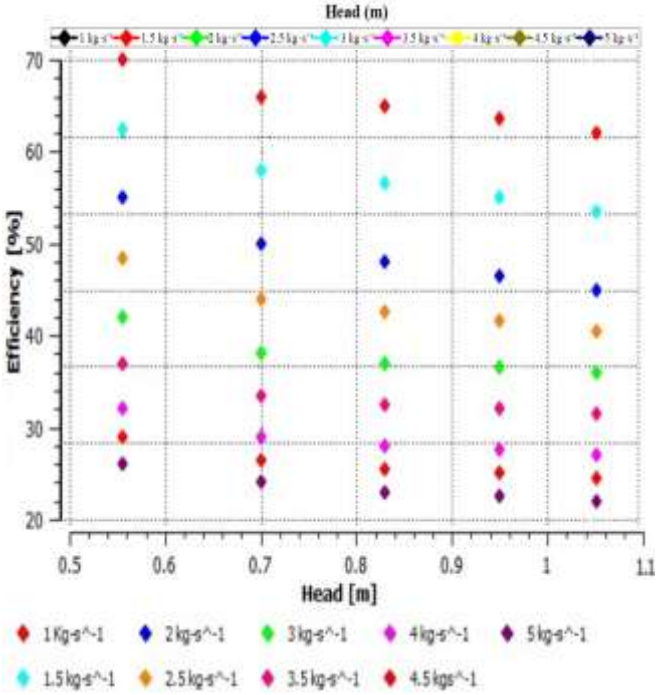


Fig. 13. Head vs Efficiency (Experimental).

Fig. 14. Head vs Efficiency (CFD).

3.1.6 Effect of Flow rate on Torque

The torque remains almost constant across all flow rates for each inclination angle, indicating that it is mainly influenced by the applied load rather than flow variation. The CFD results closely align with the experimental observations, demonstrating strong agreement and validating the reliability of the numerical model in capturing torque behaviour as depicted in Figure 15 and 16.

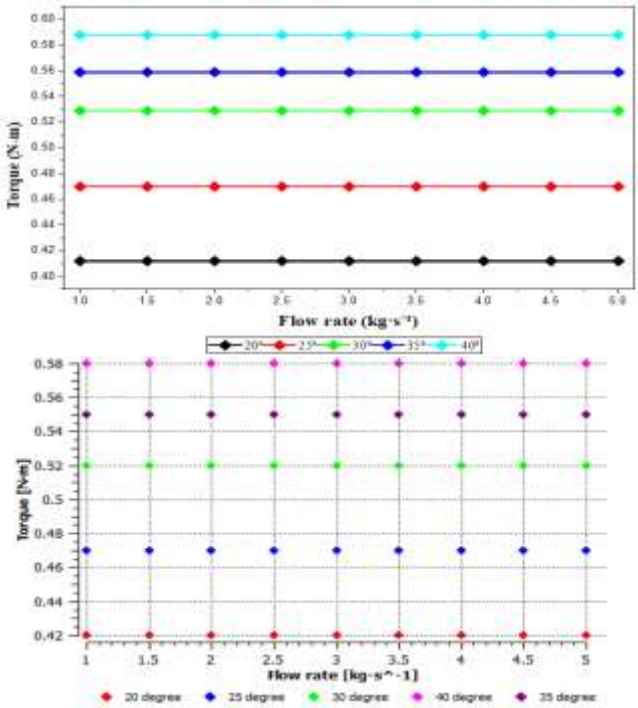
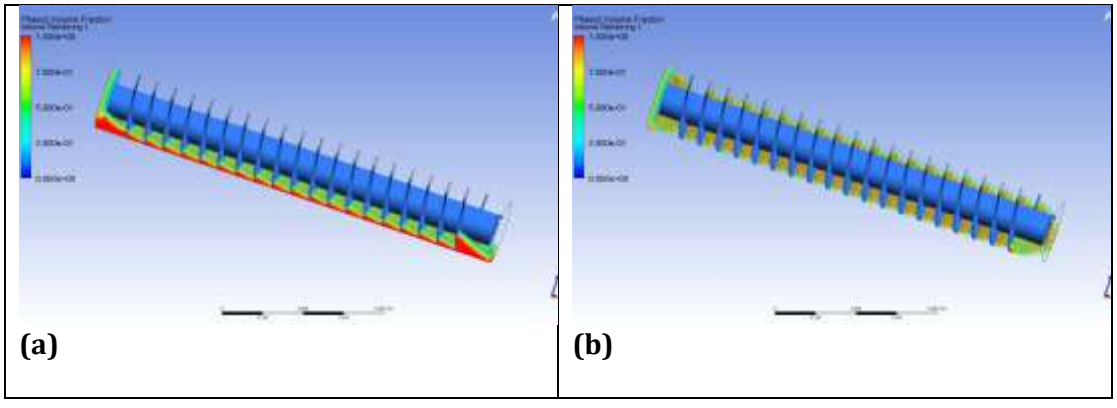


Fig. 15. Flow rate vs Torque (Experimental).

Fig. 16. Flow rate vs Torque (CFD).

3.2. Experimental and CFD analysis for flow behaviour

The results from the CFD model shows the progressive formation of flow within the AST at a flow rate of 1 kg·s^{-1} and at inclination angle of 20° which is the condition for the optimum efficiency as can be seen in Figure 17. The simulation results shows that the contours of water volume fraction capture the progressive filling of the screw chambers leading to formation of a continuous helical water column from the inlet toward the outlet. In early stages (a-c), there is incomplete filling and less contact between fluid and blade, whereas in later stages (d-f), there is complete chamber filling and continuous water motion. This behaviour shows good retention of the water in the helical channels and smooth hydrostatic behaviour with little recirculation or flow separation. The stabilisation of a continuous water column shows evidence of good fluid interaction and smooth energy transfer to the screw rotor.



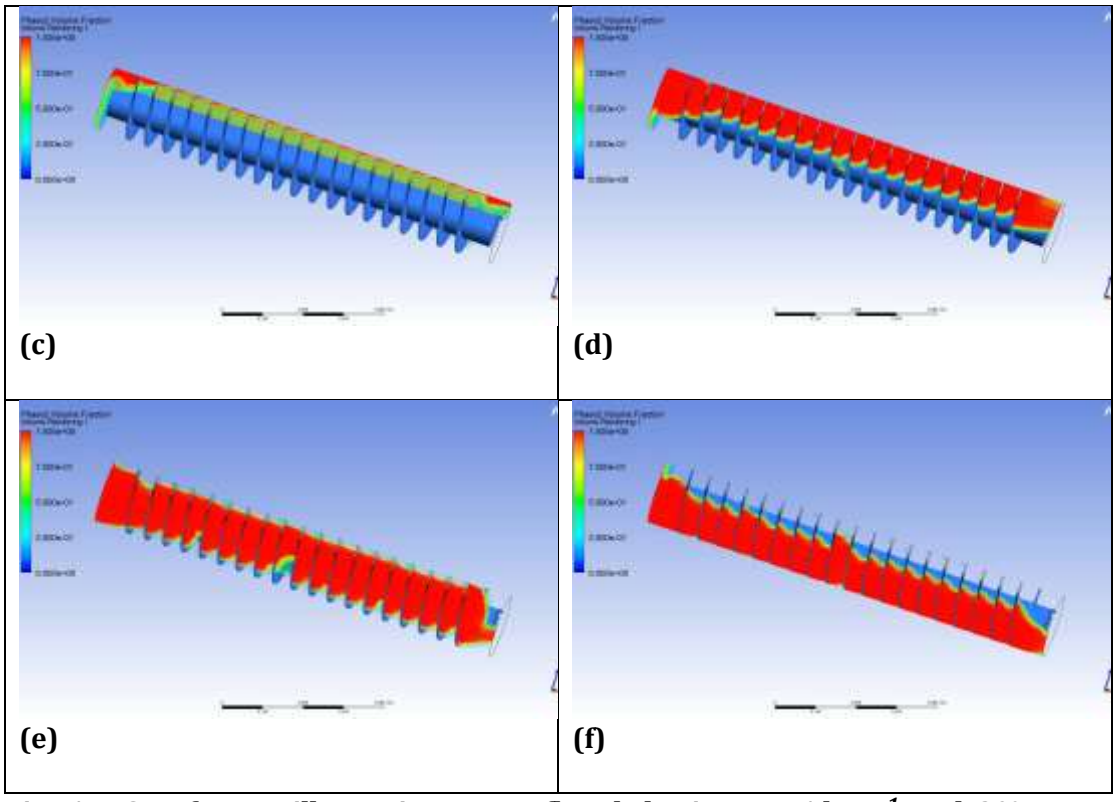


Fig. 17. CFD frames illustrating water flow behaviour at 1 kg·s^{-1} and 20° screw inclination corresponding to the condition of peak efficiency

4. Contour Analysis for AST

The AST shows a specific pressure distribution pattern which moves from the inlet to the outlet section reflecting the conversion of hydraulic power into mechanical energy. The inlet surface experiences highest pressure where the water first interacts with the blades and gradually decreases along the helical channel toward the outlet as energy is transferred to the rotor as can be seen in Figure 18. The red regions near the inlet represent the highest hydraulic head and available energy for conversion at 1 kg/s flow rate and 20° inclination angle. The flow shows efficient transformation of hydraulic potential energy into rotational mechanical energy because the pressure decreases toward the outlet (blue regions). The GI runner maintains a stable pressure field along its blade surface due to balanced hydraulic loading which allows smooth and continuous rotation. Similar formations that show significant differences between the blade areas are usually seen in the inner section of the pressure contour in Figure 19, these specific pressure variations validate efficient torque generation and water confinement along the screw length.

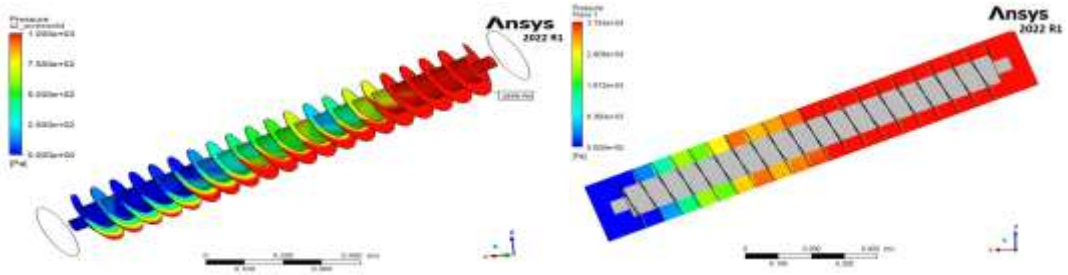


Fig. 18. Pressure distribution on outer surface ***Fig. 19. Pressure contour on inner section***

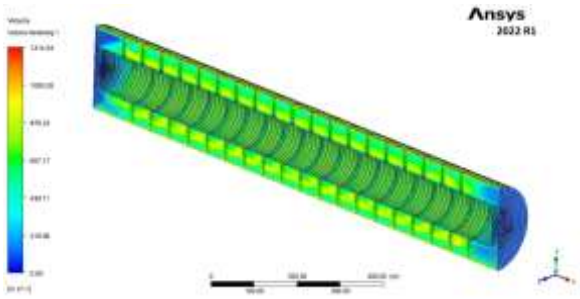


Fig. 20. Velocity distribution around AST showing inverse pressure-velocity behaviour and mild turbulence near the blade edges.

The formation of relatively small high-pressure regions at the blade edges indicates areas of intense hydraulic stress which is important for determining overall durability and material performance. The smooth pressure gradient validates the effectiveness of fluid structure interaction and shows that turbulence remains restricted to specific zones of the fluid domain. CFD results demonstrates mild turbulence intensity located within the blade edges and inter-blade paths, where confined vortices steadily dissipate downstream through the helical channel, causing little energy loss. Overall, the flow appears laminar throughout the screw length ensuring steady hydraulic performance as well as effective conversion of energy. As the pressure lowers, the velocity distribution inside the fluid region rises. Higher velocities are found near the blade edges and at the intake, whereas lower velocities are recorded downstream owing to flow expansion and extraction of energy. Mild turbulence in the higher velocity regions, as depicted in Figure 20, aligns with the shear-induced effects, demonstrating that turbulence occurs on small-scale and has no impact on entire flow stability. This inverse relationship between pressure and velocity demonstrates the efficient hydraulic performance of the screw turbine and validates the effectiveness of energy conversion from the fluid to mechanical domain. The close agreement between CFD predictions and experimental observations confirms the reliability of the simulation approach. Overall, the results indicate that under optimized flow rate and inclination conditions, the GI-based Archimedes screw turbine exhibits stable hydrodynamic behaviour, efficient hydraulic-to-mechanical energy conversion and reliable structural performance. These findings confirm the turbine suitability for small-scale, low-head hydropower applications and highlight its potential as a sustainable and cost-effective renewable energy solution.

Besides its superior hydraulic performance, the GI runner demonstrated high mechanical stability throughout experimental testing. It maintained its structural strength and balance during operation, showing strong durability and minimal deformation under load. Additionally, no corrosion or surface damage was observed after continuous water exposure showing the protective effect of GI coating. The efficiency data and CFD findings also indicated less frictional resistance between the running water and the runner surface which was appropriate with the recorded pressure and velocity gradients. These outcomes suggest the use of GI as a reliable, low-cost and durable alternative for small scale hydro power systems.

Conclusion

The study evaluates hydraulic performance of an AST with GI runner under low-head micro-hydropower systems through experimental testing and CFD simulation. The

turbine was operated under different flow rates and inclination angles to effectively evaluate its performance. The adopted methodology demonstrated its reliability through the results obtained from both experimental and numerical methods. The experimental data revealed that the turbine achieved its peak efficiency at 72.51% when operating at $1kg{\cdot}s^{-1}$ flow rate and 20° inclination angle, while numerical results confirmed 70% efficiency under identical conditions, demonstrating reliability of both approaches. The results showed that the turbine performance improved at lower angle of inclination and lower flow rates, as these conditions enabled smooth water entry and stable rotational motion which resulted in maximum hydraulic energy conversion. The pressure, velocity and turbulence distribution maintained a stable hydraulic flow pattern that minimized high-velocity zones and low turbulence intensity to achieve optimal energy transfer through the screw channel.

The galvanized iron runner demonstrated good corrosion resistance, mechanical stability and minimal frictional losses making it a durable and cost-effective alternative. The results revealed that the GI based AST operate effectively under low-head conditions which makes them appropriate for rural and decentralized hydropower systems that need affordable and reliable operations. Therefore, the study successfully achieved its objectives by proving galvanized iron as a practical, cost-effective and environmentally friendly solution for AST applications in small scale low-head micro-hydropower systems.

Future studies should focus on maximizing turbine efficiency by optimizing alternative lightweight composite materials which enables to achieve better performance and longer lifespan with lower production expenses. Integrating AST with hybrid renewable power systems that include solar and wind energy to enhance power reliability in locations without access to the main power grid offers promising direction for further research. Also, use of machine learning and AI algorithms can be employed to enhance performance and accelerate design development process.

References

[1] A. M. Omer, “Energy, environment and sustainable development,” Renewable and Sustainable Energy Reviews, vol. 12, no. 9, pp. 2265–2300, 2008, doi: 10.1016/j.rser.2007.05.001.

[2] S. H. Mohr, J. Wang, G. Ellem, J. Ward and D. Giurco, “Projection of world fossil fuels by country,” Fuel, vol. 141, pp. 120–135, 2015, doi: 10.1016/j.fuel.2014.10.030.

[3] F. Martins, C. Felgueiras, and M. Smitková, “Fossil fuel energy consumption in European countries,” Energy Procedia, vol. 153, pp. 107–111, 2018, doi: 10.1016/j.egypro.2018.10.050.

[4] S. D. Kamadje, N. S. Nouadjep and E. B. Gueguim Kana, “Assessing renewable energy trends: A global bibliometric analysis of biomass, solar, wind and geothermal resources with emphasis on Cameroon,” International Journal of Energy and Water Resources, pp. 1–20, 2025, doi: 10.1007/s42108-025-00383-7.

[5] K. E. Okedu, B. C. Oyinna, E. O. Diemuodeke, I. Colak and A. Kalam, “Multicriteria GIS-based assessment of biomass energy and hydropower potentials in Nigeria,” Measurement: Sensors, vol. 33, p. 101243, 2024, doi: 10.1016/j.measen.2024.101243.

[6] Z. Wang, T. Wang, X. Zhang, J. Wang, Y. Yang, Y. Sun, X. Guo, Q. Wu, E. Nepovimova, A. E. Watson, and K. Kuca, “Biodiversity conservation in the context of climate change: Facing challenges and management strategies,” Science of the Total Environment, vol. 937, p. 173377, 2024, doi: 10.1016/j.scitotenv.2024.173377.

[7] S. Thapa, R. Kumar, K. Kumar, S. Samir, D. Lee and T. Singh, "Analytical investigation of solar parabolic trough receiver with multiple twisted tapes using exergy and energy analysis," Case Studies in Thermal Engineering, vol. 50, p. 103493, 2023, doi: 10.1016/j.csite.2023.103493.

[8] R. Kumar, S. Kumar, Ü. Ağbulut, A. E. Gürel, M. Alwetaishi, S. Shaik, C. A. Saleel and D. Lee, "Parametric optimization of an impingement jet solar air heater for active green heating in buildings using hybrid CRITIC–COPRAS approach," International Journal of Thermal Sciences, vol. 197, p. 108760, 2024, doi: 10.1016/j.ijthermalsci.2023.108760.

[9] T. Kashyap, B. Sharma and N. Sharma, "Design and simulation of PEDOT:PSS and P3HT:PCBM based HIT solar cell to improve the internal quantum efficiency," International Research Journal of Engineering and Technology, vol. 8, no. 5, 2021.

[10] R. Kumar, M. Sethi, V. Goel, M. K. Ramis, M. AlSubih, S. Islam, M. S. A. Ansari, D. Lee and A. W. Wodajo, "Thermal and effective assessment of solar thermal air collector with roughened absorber surface: An analytical examination," International Journal of Low Carbon Technologies, vol. 19, pp. 1112–1123, 2024, doi: 10.1093/ijlct/ctae056.

[11] S. Aggarwal, R. Kumar, S. Kumar and T. Singh, "Impact of fin material properties and the inclination angle on the thermal efficiency of evacuated tube solar water heater: an experimental study," Journal of King Saud University Science, vol. 36, p. 103186, 2024, doi: 10.1016/j.jksus.2024.103186.

[12] A. K. Yadav, R. Khargotra, D. Lee, R. Kumar and T. Singh, "Novel applications of various neural network models for prediction of photovoltaic system power," Sustainable Energy, Grids and Networks, vol. 38, p. 101318, 2024, doi: 10.1016/j.segan.2024.101318.

[13] S. Kumar, R. Kumar, R. Thakur, S. Kumar and D. Lee, "Effects of climate variables and nanofluid-based cooling on the efficiency of a liquid spectrum filter-based concentrated photovoltaic thermal system," Journal of Thermal Analysis and Calorimetry, vol. 149, pp. 2273–2291, 2024, doi: 10.1007/s10973-023-12836-4.

[14] S. Kumar, R. Thakur, S. Kumar, D. Lee and R. Kumar, "Impact of liquid spectrum filter and solar tracker on the overall effectiveness of a photovoltaic thermal system," Renewable Energy, vol. 226, p. 120390, 2024, doi: 10.1016/j.renene.2024.120390.

[15] N. Girgibo, E. Hiltunen, X. Lü, A. Mäkiranta and V. Tuomi, "Risks of climate change effects on renewable energy resources and the effects of their utilisation on the environment," Energy Reports, vol. 11, pp. 1517–1534, 2024, doi: 10.1016/j.egyr.2024.01.024.

[16] S. U. Batgi and I. Dincer, "Design of a two-renewable energy source-based system with thermal energy storage and hydrogen storage for sustainable development," Journal of Energy Storage, vol. 89, p. 111742, 2024, doi: 10.1016/j.est.2024.111742.

[17] T. Song and J. Teh, "Coordinated integration of wind energy in microgrids: A dual strategy approach leveraging dynamic thermal line rating and electric vehicle scheduling," Sustainable Energy, Grids and Networks, vol. 38, p. 101299, 2024, doi: 10.1016/j.segan.2024.101299.

[18] J. K. Babu, L. Rajesh, A. M. Sarma and M. S. Ganesh, "Hybrid power generation from waste by integrating solar, hydel and TEG module," Proceedings of the 7th International Conference on Inventive Material Science and Applications, pp. 593–598, 2025, doi: 10.1109/ICIMA64861.2025.11073902.

[19] Z. Wang, F. K. Chan, M. Feng and M. F. Johnson, "Greenhouse gas emissions from hydropower reservoirs: Emission processes and management approaches," Environmental Research Letters, vol. 19, no. 7, p. 073002, 2024, doi: 10.1088/1748-9326/ad560c.

[20] T. H. Bakken, H. Sundt, A. Ruud and A. Harby, "Development of small versus large hydropower in Norway: Comparison of environmental impacts," Energy Procedia, vol. 20, pp. 185–199, 2012, doi: 10.1016/j.egypro.2012.03.019.
[21] T. S. Aung, T. B. Fischer and A. S. Azmi, "Are large-scale dams environmentally detrimental? Life-cycle environmental consequences of mega-hydropower plants in Myanmar," International Journal of Life Cycle Assessment, vol. 25, no. 9, pp. 1749–1766, 2020, doi: 10.1007/s11367-020-01795-9.
[22] T. Kashyap, R. Thakur, G. H. Ngo, D. Lee, G. Fekete, R. Kumar and T. Singh, "Silt erosion and cavitation impact on hydraulic turbines performance: An in-depth analysis and preventative strategies," Heliyon, vol. 10, no. 8, 2024, doi: 10.1016/j.heliyon.2024.e28998.
[23] Y. Xiao, L. He, X. Chen, Z. He, Y. Lai, F. Luo, Y. Cen, D. Li and R. Jin, "Impacts of large hydropower projects on the ecological environment of watersheds: A case study of Ertan reservoir area," Sustainability, vol. 16, no. 20, p. 9125, 2024, doi: 10.3390/su16209125.
[24] L. Li, Y. Wu, Y. Han, Z. Xu, X. Wu, Y. Luo, and J. Shen, "Problems and strategies for maintenance scheduling of a giant cascaded hydropower system in the Lower Jinsha River," Energies, vol. 18, no. 14, p. 3831, 2025, doi: 10.3390/en18143831.
[25] H. B. Lamesgin and A. N. Ali, "Optimization of screw turbine design parameters to improve the power output and efficiency of micro-hydropower generation," Cogent Engineering, vol. 11, no. 1, p. 2327906, 2024, doi: 10.1080/23311916.2024.2327906.
[26] A. Allouhi, "A hybrid PV/wind/battery energy system to assist a run-of-river micro-hydropower for clean electrification and fuelling hydrogen mobility for young population in a rural Moroccan site," Journal of Cleaner Production, vol. 442, p. 140852, 2024, doi: 10.1016/j.jclepro.2024.140852.
[27] A. M. Daabo, A. Basem, M. Zafar, A. Alkhabbaz, A. Ahmad, Q. R. Al-Amir, H. K. Easa and H. K. Ahmad, "A novel design of a hybrid micro-scale multistage turbine model for sustainable energy sources," Case Studies in Thermal Engineering, p. 106873, 2025, doi: 10.1016/j.csite.2025.106873.
[28] M. A. Khan, A. U. Rehman and I. U. Rehman, "An assessment of the cost-effectiveness and environmental sustainability of mini micro hydro power projects in Khyber Pakhtunkhwa, Pakistan," The Sciencetech, vol. 6, no. 2, pp. 85–97, 2025.
[29] N. Triana, N. Mukhtar, O. M. Rasip, H. F. Ramadhan and L. J. Monk, "Legal system of community participation in environmentally friendly power plants: A socio-legal study of micro-hydro projects in Central Java," Jurnal Hukum, vol. 41, no. 3, pp. 567–587, 2025, doi: 10.26532/jh.41.3.567-587.
[30] J. S. Jeong, S. K. Lim and S. W. Lee, "Aerodynamic performance of suction-side squealer tip in impulse/reaction turbine blade rows," Experimental Thermal and Fluid Science, vol. 136, p. 110666, 2022, doi: 10.1016/j.expthermflusci.2022.110666.
[31] M. Alonso-Martinez, J. L. Suárez Sierra, J. J. Coz Díaz and J. E. Martinez-Martinez, "A new methodology to design sustainable Archimedean screw turbines as green energy generators," International Journal of Environmental Research and Public Health, vol. 17, no. 24, p. 9236, 2020, doi: 10.3390/ijerph17249236.
[32] R. Thakur, T. Kashyap, R. Kumar, R. K. Saini, D. Lee, S. Kumar and T. Singh, "Potential of the Archimedes screw to generate sustainable green energy for mini, micro, and pico hydro turbine power stations: An extensive analysis," Energy Strategy Reviews, vol. 55, p. 101514, 2024, doi: 10.1016/j.esr.2024.101514.
[33] I.S. Pauwels, J. Tuhtan, J. Coeck and D. Baeyens, "Archimedes screw – an alternative for safe migration through turbines?," Novel Developments for Sustainable

Hydropower, Cham: Springer International Publishing, pp. 125–133, 2022, doi: 10.1007/978-3-030-99138-8_11.
[34] P. Koukouvinis and J. Anagnostopoulos, "State of the art in designing fish-friendly turbines: Concepts and performance indicators," Energies, vol. 16, no. 6, p. 2661, 2023, doi: 10.3390/en16062661.
[35] A.T. Ubando, I. A. Marfori III, M. S. Peradilla, C. L. Sy, A. M. Calapatia and W. H. Chen, "Sustainable manufacturability of Archimedes screw turbines: A critical review," Journal of Manufacturing and Materials Processing, vol. 6, no. 6, p. 161, 2022, doi: 10.3390/jmmp6060161.
[36] H. Helmizar, N. Windiharto, Y. Witanto, A. K. Mainil, R. I. Mainil and K. Sai, "Experimental study on a laboratory-scale Archimedes screw turbine using pitch-to-diameter ratio for low-head hydropower," Jurnal Polimesin, vol. 23, no. 3, pp. 301–307, 2025, doi: 10.30811/jpl.v23i3.6690.
[37] B. Indarto, D. N. Kumalasari and M. A. Bustomi, "Archimedean screw-based micro hydro power plant prototype with turbine elevation angle parameters," Journal of Physics: Conference Series, vol. 2623, p. 012026, 2023, doi: 10.1088/1742-6596/2623/1/012026.
[38] M. I. Maulana, R. Sary, A. Syuhada, S. Mayasari and Y. Yusmanizar, "Investigation of pressure distribution in an Archimedes screw turbine with head below one meter using CFD," Jurnal Polimesin, vol. 22, no. 2, pp. 252–257, 2024, doi: 10.30811/jpl.v22i2.4901.
[39] B. Darmono and H. Pranoto, "Archimedes screw turbines performance analysis using CFD software based on variation of blades distance and thread number on the pico hydropower plant," International Journal of Advanced Technology in Mechanical, Mechatronics and Materials, vol. 3, no. 1, pp. 18–25, 2022, doi: 10.37869/ijatec.v3i1.53.
[40] V. Uniyal, A. Karn and V. P. Singh, "Parametric optimization of Archimedes screw turbine by response surface methodology and artificial neural networks," Renewable Energy and Sustainable Development, vol. 10, no. 2, pp. 100–108, 2024, doi: 10.21622/RESD.2024.10.2.1008.
[41] I. Imawati, M. Febiansyah, E. K. Novtrianda and H. Mubarok, "Portable pico-hydro power plant with Archimedes screw turbine in Pelangi reservoir of Universitas Islam Indonesia," ELKHA: Jurnal Teknik Elektro, vol. 14, no. 2, pp. 132–138, 2022, doi: 10.26418/elkha.v14i2.57770.
[42] K. Muzaka, D. R. Pamuji, M. A. Wahid, S. Hadi and J. D. Prasetyo, "Effect of Archimedes screw turbine shaft inclination on output power," International Journal of Software and Hardware Research in Engineering, vol. 9, no. 3, 2021, doi: 10.26821/IJSHRE.9.3.2021.9314.
[43] D. S. Edirisinghe, H. S. Yang, M. S. Kim, B. H. Kim, S. P. Gunawardane and Y. H. Lee, "Computational flow analysis on a real-scale run-of-river Archimedes screw turbine with a high incline angle," Energies, vol. 14, no. 11, p. 3307, 2021, doi: 10.3390/en14113307.
[44] M. Zamani, R. Shafaghat and B. A. Kharkeshi, "Numerical study of the hydrodynamic behavior of an Archimedes screw turbine by experimental data in order to optimize turbine performance: the genetic algorithm," Journal of Applied and Computational Mechanics, vol. 9, no. 4, pp. 1060–1075, 2023, doi: 10.22055/jacm.2023.43137.4031.
[45] K. Kashyap, R. Thakur, S. Kumar and R. Kumar, "Identification of Archimedes screw turbine for efficient conversion of traditional water mills into micro hydropower stations in western Himalayan regions of India," International Journal of Renewable Energy Research, vol. 10, no. 3, pp. 1451–1463, 2020.

[46] M. D. Lee and P. S. Lee, "Modelling the energy extraction from low-velocity stream water by small-scale Archimedes screw turbine," Journal of King Saud University – Engineering Sciences, vol. 35, no. 5, pp. 319–326, 2023, doi: 10.1016/j.jksues.2021.04.006.

[47] Z. Abbas, M. Waqas, S. S. Khan, R. Khatoon, S. Larkin and L. Zhao, "Numerical and experimental investigation of an Archimedes screw turbine for open channel water flow application," Energy Science and Engineering, vol. 12, no. 4, pp. 1317–1336, 2024, doi: 10.1002/ese3.1649.

[48] K. Shahverdi, R. Loni, J. M. Maestre and G. Najafi, "CFD numerical simulation of Archimedes screw turbine with power output analysis," Ocean Engineering, vol. 231, p. 108718, 2021, doi: 10.1016/j.oceaneng.2021.108718.

[49] O. S. Abdullah, W. H. Khalil, A. H. Kamel and A. J. Shareef, "Investigation of physical and numerical model of Archimedes screw turbine," Journal of Power and Energy Engineering, vol. 8, no. 10, pp. 26–42, 2020, doi: 10.4236/jpee.2020.810003.

[50] A. YoosefDoost and W. D. Lubitz, "Development of an equation for the volume of flow passing through an Archimedes screw turbine," In Sustaining Tomorrow: Proceedings of Sustaining Tomorrow 2020 Symposium and Industry Summit, Cham: Springer International Publishing, pp. 17–37, 2021, doi: 10.1007/978-3-030-64715-5_2.

[51] S. Simmons, G. Dellinger, M. Lyons, A. Terfous, A. Ghenaim and W. D. Lubitz, "Effects of inclination angle on Archimedes screw generator power production with constant head," Journal of Hydraulic Engineering, vol. 147, no. 3, p. 04021001, 2021, doi: 10.1061/(ASCE)HY.1943-7900.0001854.

[52] A. I. Siswantara, M. H. Syafei, M. A. Budiyanto, C. D. Widiawaty, A. Syuriadi and T. A. Farhan, "Design of Archimedes screw turbine: Exploring the influence of pitch ratio, radius ratio, and inclination angle on outer diameter size," Cogent Engineering, vol. 11, no. 1, p. 2389685, 2024, doi: 10.1080/23311916.2024.2389685.

[53] D. S. Pillai, C. Stephen, D. K. Tiwari and M. Singh, "Onsite performance testing of Archimedes hydropower screw for low head and ultra-low head hydropower project – A case study," IOP Conference Series: Earth and Environmental Science, vol. 1411, no. 1, p. 012070, 2024, doi: 10.1088/1755-1315/1411/1/012070.

[54] T. F. Ardiansyah, M. I. Maulana and A. Syuhada, "The influence of incoming water flows and head variations on the Archimedes screw turbine torque force for low head hydroelectric power plants," Defect and Diffusion Forum, vol. 441, pp. 117–124, 2025, doi: 10.4028/p-B5l2xS.

[55] Z. Abbas, M. Waqas, S. S. Khan, R. Khatoon, S. Larkin and L. Zhao, "Numerical and experimental investigation of an Archimedes screw turbine for open channel water flow application," Energy Science and Engineering, vol. 12, no. 4, pp. 1317–1336, 2024, doi: 10.1002/ese3.1649.

[56] N. Khan, M. K. Sarwar, M. Rashid, H. K. Abbasi, S. Haider, M. A. Tariq, A. Nadeem, M. A. Zulfiqar, A. Salem, N. Al-Ansari and A. M. Okasha, "Development of a sustainable portable Archimedes screw turbine for hydropower generation," Scientific Reports, vol. 15, no. 1, p. 5827, 2025, doi: 10.1038/s41598-025-90634-8.